Title	Al L-2,L-3 edge x-ray absorption spectra in III-V semiconductors: Many-body perturbation theory in comparison with experiment
Author(s)	Olovsson, W.; Tanaka, I.; Mizoguchi, T.; Radtke, G.; Puschnig, P.; Ambrosch-Draxl, C.
Citation	PHYSICAL REVIEW B (2011), 83(19)
Issue Date	2011-05
URL	http://hdl.handle.net/2433/161787
Right	©2011 American Physical Society
Type	Journal Article
Textversion	publisher

Al $L_{2,3}$ edge x-ray absorption spectra in III-V semiconductors: Many-body perturbation theory in comparison with experiment

W. Olovsson,[1,2] I. Tanaka,[2,3] T. Mizoguchi,[4] G. Radtke,[5] P. Puschnig,[1] and C. Ambrosch-Draxl[1]

[1]*Chair of Atomistic Modelling and Design of Materials, Montanuniversität Leoben, Franz-Josef-Straße 18, A-8700 Leoben, Austria*

[2]*Department of Materials Science and Engineering, Kyoto University, Sakyo, Kyoto 606-8501, Japan*

[3]*Nanostructures Research Laboratory, Japan Fine Ceramics Centre, Atsuta, Nagoya 456-8587, Japan*

[4]*Institute of Industrial Science, The University of Tokyo, 4-6-1, Komaba, Meguro, Tokyo 153-8505, Japan*

[5]*IM2NP, UMR 6242 CNRS, Faculté des Sciences de Saint-Jérôme, Université Aix-Marseille III, Case 262, F-13397 Marseille cedex 20, France*

(Received 10 December 2010; revised manuscript received 25 March 2011; published 9 May 2011)

We investigate core excitations of the Al $2p$ edge in the III-V semiconductors AlP, AlAs, AlSb, and AlN. For the latter, we consider the wurtzite, zinc-blende, and rock-salt polymorphs. First-principles calculations are performed utilizing two different approaches, which are the solution of the Bethe-Salpeter equation (BSE) as well as the supercell technique employing the core-hole approximation. In addition, measurements of the electron energy-loss near-edge structure of the metastable AlN phase are presented. We find that the relative intensities of the spectral features are better described by the BSE than by the supercell method. We analyze the character of the near-edge peaks and trace back their origin to strongly bound core excitons in the case of AlSb and rock-salt AlN.

DOI: 10.1103/PhysRevB.83.195206 PACS number(s): 71.15.−m, 71.35.−y, 78.70.Dm

I. INTRODUCTION

III-V semiconductors are important materials in electronic and optoelectronic devices.[1] Aluminum III-V compounds have, for instance, been used to form heterostructures with gallium III-V compounds such as GaN, GaP, and GaAs. Therefore understanding their fundamental properties is not only of academic interest, but also in view of possible future applications. AlN is stable in the wurtzite (w) phase, while the zinc-blende (zb) structure is metastable, and the rock-salt (rs) structure can only be reached under high-pressure conditions. In contrast, AlP, AlAs, and AlSb form the zinc-blende structure under ambient conditions.

X-ray absorption near-edge structure (XANES) and electron energy-loss near-edge structure (ELNES) are widely used spectroscopy techniques to probe the excited states in a material.[2–8] Due to the sensitivity of the spectral response to the atomic environment valuable chemical information can be obtained. The measured spectra can be used as a *fingerprint* for structural characterization and for identifying the constituent atoms in a material. In order to quantitatively reproduce the spectral features and understand the origin of the underlying electronic excitations, it is vital to use adequate theoretical methods.

Over the last years, there has been an increased activity to theoretically describe XANES, ELNES, and related spectroscopies.[9–20] As excitonic effects can dominate the near-edge absorption spectra of insulating solids, the core hole needs to be carefully accounted for. In most methods based on density-functional theory (DFT), such as the real-space Green-function method[21] and different supercell techniques,[22–24] this is done by including a localized core hole into the self-consistent calculations. A different approach is to consider the correlated motion of the excited electron and the hole in the absorption process. This is done by solving the equation of motion for the electron-hole (e-h) two-particle Green function, the Bethe-Salpeter equation (BSE)[25–31] within many-body perturbation theory. BSE has been successfully applied to study the x-ray absorption spectra of several materials,[9–14] and is expected to become more widespread with the availability of open-source codes.[32,33] While for wurtzite AlN the optical and the x-ray range have been investigated within the BSE formalism,[7,34,35] theoretical work on the Al-$L_{2,3}$ edge[36–39] has been based on the supercell technique.

In this work, we investigate core excitations from the Al-$L_{2,3}$ edge in AlN, AlP, AlAs, and AlSb by performing BSE calculations. For comparison, we present results from the supercell approach. We compare the outcome of both techniques with experiment. While ELNES spectra for the wurtzite and the rock-salt structures of AlN are taken from literature, we include measurements for the metastable zinc-blende phase.

II. THEORY

We solve the Bethe-Salpeter equation[25–31] for the electron-hole pair Green function within an all-electron framework. The present scheme is based on the full-potential linearized augmented plane-wave (FPLAPW) method[40] as implemented in the WIEN2K program package[41] to obtain the single-particle energies and wave functions as a starting point. The corresponding solution of the BSE is described in Ref. 42. It has previously been used to obtain the optical spectra in different materials[35,43–46] and was applied for the shallow core edges Li-K and Mg-$L_{2,3}$.[13,14] A short summary of the methodology[25,42] is given below.

By expressing the two-particle electron-hole Green function in terms of single-particle electron and hole wave functions, the Bethe-Salpeter equation can be transformed into a matrix eigenvalue equation,

$$\sum_{\alpha'\beta'\mathbf{k}'} H^{\mathrm{eh}}_{\alpha\beta\mathbf{k},\alpha'\beta'\mathbf{k}'} A^{\lambda}_{\alpha'\beta'\mathbf{k}'} = E^{\lambda} A^{\lambda}_{\alpha\beta\mathbf{k}}, \tag{1}$$

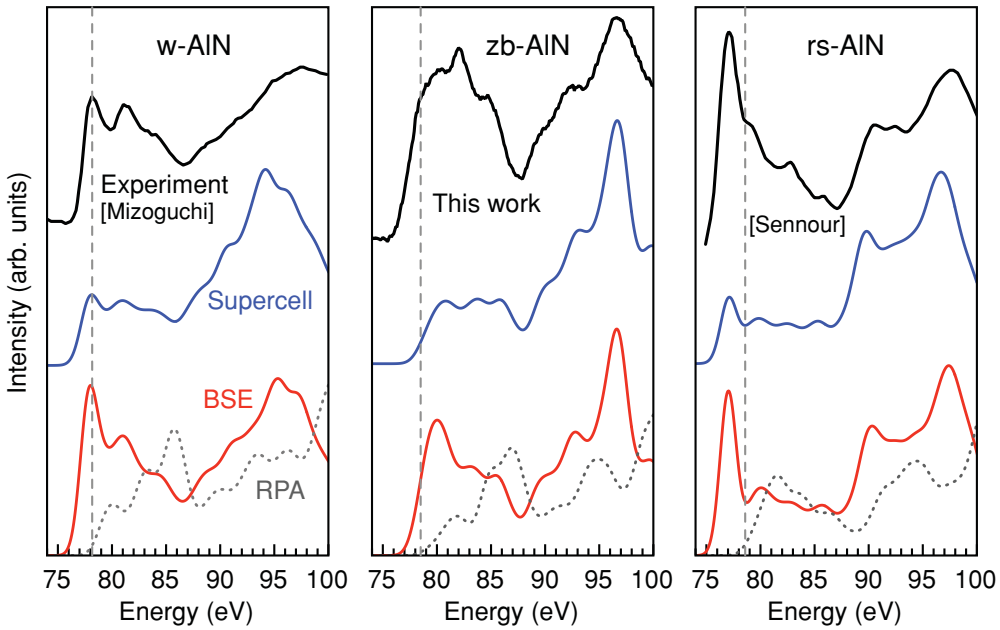

FIG. 1. (Color online) Near-edge absorption spectra for the Al-$L_{2,3}$ edge in different polymorphs of AlN, i.e., from left to right, wurtzite, zinc-blende, and rock-salt structure. Dashed vertical lines mark the reference for bound core excitons. Measurements are shown as bold black lines (top), where the data for w- and rs-AlN are taken from literature (Refs. 38 and 52). Blue (middle) and red (bottom) lines, respectively, indicate the theoretical spectra obtained from the supercell approach and the BSE calculation. RPA results including local-field effects are displayed as gray dotted lines.

where α and β correspond to initial and final states, respectively, and $\mathbf{k}$ is a wave vector inside the first Brillouin zone. H^{eh} is the effective *e-h* two-particle Hamiltonian, while λ enumerates the excitations with eigenenergies E^{λ} and eigenvectors $A^{\lambda}_{\alpha\beta\mathbf{k}}$, interpreted as coupling coefficients for the *e-h* pairs. Neglecting spin-orbit coupling results in the Hamiltonian for spin-singlet excitations,

$$H^{\mathrm{eh}} = H^{\mathrm{diag}} + H^{\mathrm{dir}} + 2H^{\mathrm{x}}. \tag{2}$$

Here, H^{diag} is the diagonal term, which corresponds to the differences between electron and hole energies. H^{dir} is the direct term involving the static screened Coulomb interaction, which is responsible for the creation of bound core-exciton states. H^{x} is the exchange term, which contains the unscreened short-range Coulomb interaction and accounts for local-field effects. The photon absorption is described in terms of the imaginary part of the dielectric function,

$$\epsilon_2(\omega) \propto \sum_{\lambda} \left| \sum_{\alpha\beta\mathbf{k}} A^{\lambda}_{\alpha\beta\mathbf{k}} \frac{\langle \beta\mathbf{k}|p|\alpha\mathbf{k}\rangle}{\varepsilon_{\beta\mathbf{k}} - \varepsilon_{\alpha\mathbf{k}}} \right|^2 \times \delta(E^{\lambda} - \omega). \tag{3}$$

Here, $\varepsilon_{\alpha\mathbf{k}}$ describes the initial-state core level, $\varepsilon_{\beta\mathbf{k}}$ stands for the final valence states, and $\langle \beta\mathbf{k}|p|\alpha\mathbf{k}\rangle$ are the transition matrix elements in the electric-dipole approximation. Note that we kept the $\mathbf{k}$ dependence of the core state, as higher-lying core levels as investigated here can exhibit a small dispersion, and the sum over α refers to the two different edges, L_2 and L_3. By excluding the direct term in Eq. (2), i.e., the attractive Coulomb interaction between the electron and the hole, one obtains the random-phase approximation (RPA) including crystal local-field effects.

The exciton wave function is given by

$$\Phi^{\lambda}(\mathbf{r}_{\mathrm{e}}, \mathbf{r}_{\mathrm{h}}) = \sum_{\alpha\beta\mathbf{k}} A^{\lambda}_{\alpha\beta\mathbf{k}} \psi^{*}_{\alpha\mathbf{k}}(\mathbf{r}_{\mathrm{h}}) \psi_{\beta\mathbf{k}}(\mathbf{r}_{\mathrm{e}}), \tag{4}$$

where $\mathbf{r}_{\mathrm{e}}$ and $\mathbf{r}_{\mathrm{h}}$ denote the real-space electron and hole coordinates and ψ is the respective single-particle wave functions.

In the present BSE and RPA calculations, a shifted $8 \times 8 \times 4$ $\mathbf{k}$ mesh (40 irreducible $\mathbf{k}$ points) and 27 unoccupied states were used for w-AlN. For zb-AlN and rs-AlN, a $10 \times 10 \times 10$ mesh (73 $\mathbf{k}$ points) and a $9 \times 9 \times 9$ mesh (35 $\mathbf{k}$ points) were utilized, respectively, considering 17 conduction states in both cases. For AlP, AlAs, and AlSb, a $9 \times 9 \times 9$ $\mathbf{k}$ mesh (55 $\mathbf{k}$ points) and 23 unoccupied states were taken into account. The theoretical lattice parameters for the different phases of AlN are $a = 3.07$ and $c = 4.92$ Å for wurtzite, $a = 4.40$ Å in the zinc-blende phase, and 4.07 Å for the rock-salt structure. These values are within 1.5% of the experimental ones. For the other zinc-blende structure materials experimental lattice constants were used, i.e., $a = 5.45$ Å for AlP, 5.62 Å in AlAs, and 6.13 Å in AlSb.[47]

As an alternative to the Bethe-Salpeter approach described above, we employed the supercell technique where a hole is created at the considered core level of a single atomic site in the supercell. (We will further refer to this as the *supercell approach*.) Overall charge neutrality in the cell is ensured by inserting an additional electron into the conduction band. To avoid spurious interaction between the core-ionized atoms due to the periodic boundary conditions, it is important to have a sufficiently large supercell. Typically, a distance larger than 10 Å is needed, roughly corresponding to ~100 or more atoms in the supercell. Here we used 128 atoms for zb- and rs-AlN,

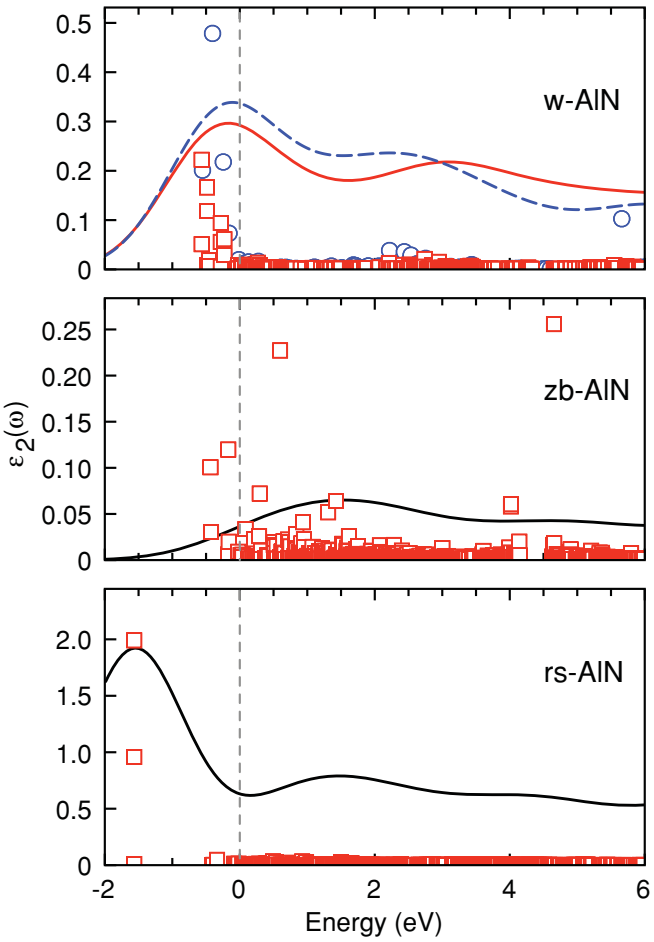

FIG. 2. (Color online) Oscillator strengths of the Al-$L_{2,3}$ edge excitations (symbols) together with the dielectric function (lines) for wurtzite, zinc-blende, and rock-salt AlN (from top to bottom). For w-AlN, both components, i.e., $\mathbf{E} \perp c$ (red boxes, full line) and $\mathbf{E} \parallel c$ (blue circles, dashed line) contributions are shown.

108 atoms for w-AlN, and 216 atoms for AlP, AlAs and AlSb, respectively.

In all DFT calculations, we employed the generalized gradient approximation (GGA) as parametrized according to Perdew *et al.*,[48] as the exchange-correlation functional. For the theoretical spectra, a Gaussian broadening of $\sigma = 0.75$ eV was applied. As the single-particle Kohn-Sham energies, in general, do not correspond to the experimental electron binding energies, the computed spectra are shifted in energy, using the experimental edges for the alignment. For the BSE results, the magnitude of this shift is of the order of 10 eV, where the individual values will be given in the Results section. To provide a consistent comparison, the same shift is applied to the RPA spectra corresponding to a scissors shift of the Kohn-Sham conduction bands.

III. EXPERIMENT

A thick film (∼300 nm) of zinc-blende AlN was grown by molecular-beam epitaxy at 720 °C on a 3C-SiC(100) substrate. The thick (∼1 μm) SiC (100) substrate employed in these experiments was previously grown by chemical vapor deposition on Si (100).[49] A cross-sectional transmission electron microscopy sample was prepared by conventional mechanical polishing to reach a thickness of about 20 μm and then thinned to electron transparency by low angle Ar ion-beam milling. The Al-$L_{2,3}$ electron energy-loss spectrum was recorded at 300 keV in diffraction mode with a collection semiangle of ∼4 mrad on a JEOL 3010 microscope equipped with a LaB_6 filament and a Gatan Imaging Filter. The thickness of the TEM sample, measured by EELS, was estimated to 30–40 nm in the area of analysis. The only post-acquisition treatments performed on the experimental Al-$L_{2,3}$ spectrum were a background subtraction using standard power-law procedures followed by a deconvolution of plural scattering using the Fourier ratio method. The energy resolution, measured as the full width at half maximum of the zero loss peak, was close to 1.1 eV. Despite the presence of a high density of hexagonal inclusions in the sample, large zones of high quality zinc-blende AlN were observed and used to record the experimental spectrum shown hereafter.

IV. RESULTS AND DISCUSSION

A. AlN polymorphs

We have investigated the Al-$L_{2,3}$ edge for three different phases of AlN: the stable wurtzite lattice, and the metastable zinc-blende and rock-salt structures. Wurtzite is characterized by interpenetrating hexagonal close-packed lattices, while zinc blende is formed from interpenetrating face-centered-cubic lattices. Though the stacking sequence is different, i.e., $ABAB$ for w and $ABCABC$ for zb, respectively, the different phases share many similarities. Both structures have a coordination number of 4, while there are six nearest neighbors in the rock-salt phase. As the wurtzite structure is anisotropic, there are two independent components in the dielectric tensor. For comparison with experiment, we describe the spectrum as the average over the different directions. The similarities between the wurtzite and zinc-blende structures give rise to comparable features in the absorption spectra, as discussed in Refs. 51, 38, and 50.

The excitation spectra for the Al $2p$ core levels are shown in Fig. 1 for the three phases. Experimental data are given in the upper parts of the figure, with the w- and rs-AlN data taken from previous ELNES measurements.[38,52] Only a few measurements have been conducted for the Al-$L_{2,3}$ edge in rock-salt AlN[52,53] and, as far as we know, there are no other experimental studies available for the AlN zinc-blende phase. Our results for the supercell technique and Bethe-Salpeter equation are given as solid blue lines (middle) and red lines (bottom), respectively. Results from the RPA (dotted lines), including local-field effects, demonstrate the effect of ignoring the attractive part of the electron-hole interaction. As mentioned before, the theoretical spectra are aligned with the experimental edge peaks by shifting the BSE results by 11.6, 13.2, and 10.6 eV for the w, zb, and rs spectra, respectively. The conduction-band minima (vertical dashed lines) are used as references for estimating the exciton binding energies. The BSE spectrum for w-AlN was briefly discussed in Ref. 7. Our supercell/core-hole spectra are similar to previous theoretical work using the orthogonalized linear combination of atomic orbitals (OLCAO) method.[38]

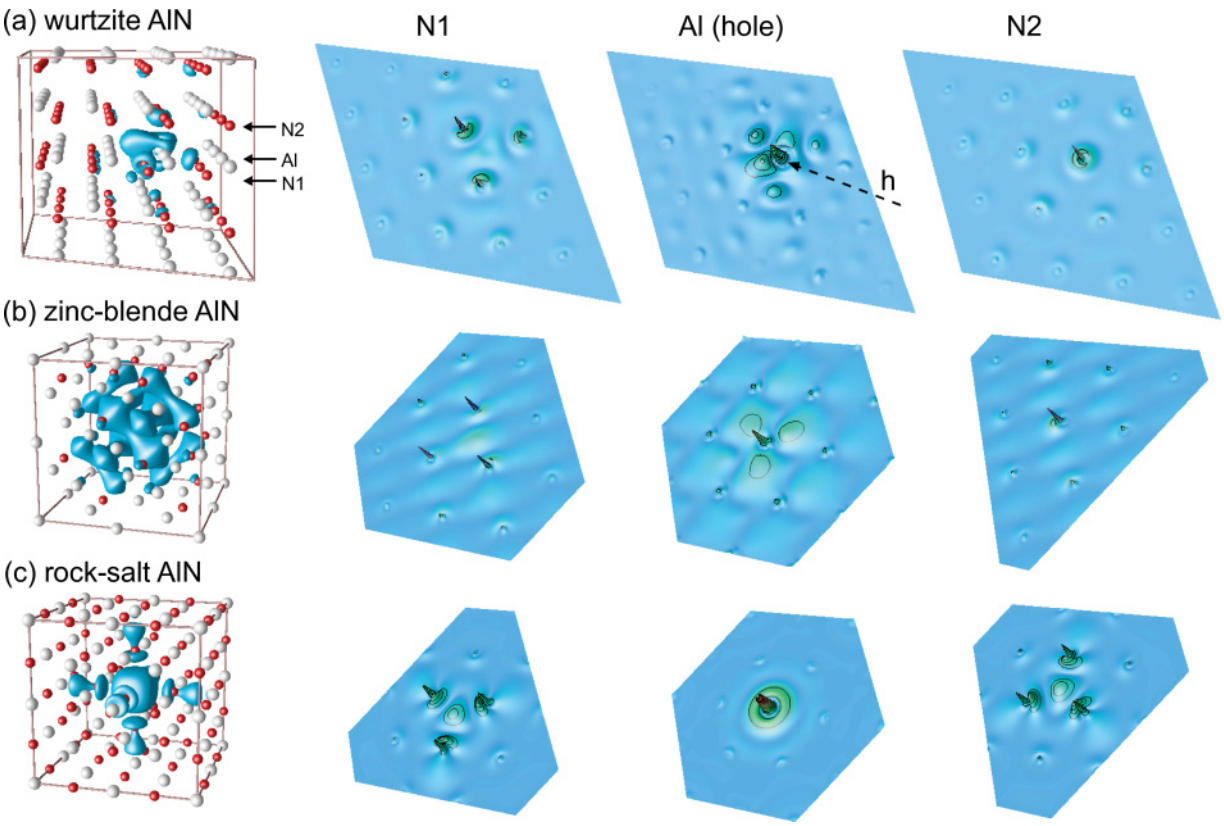

FIG. 3. (Color online) Bound core-exciton state at the Al-$L_{2,3}$ edge in AlN in (a) the wurtzite, (b) the zinc-blende, and (c) the rock-salt structure. In the left panels, the absolute value (modulus) of the wave function is depicted as isosurface inside the lattice model. The right panels represent contour plots of the electron density for three selected lattice planes through Al and neighboring nitrogen atoms, respectively, as described in the text. The symmetric patterns formed by local maxima correspond to atomic sites.

By comparing the results obtained for BSE and the supercell technique with those of RPA, we find that the intensity is radically redistributed close to the core-edge region when considering excitonic effects. This redistribution is more pronounced when treating the *e*-*h* interaction within the nonlocal BSE formalism. While the supercell approach reproduces several of the features in the spectra, there is a significant difference in the relative distribution of the intensities over the energy range. In comparison with experiment, BSE, in general, excellently reproduces the fine structure and intensity ratios over the whole energy range in all the three phases. However, both theoretical methods differ from experiment at the edge peak for zb-AlN. This discrepancy will be discussed in further detail below.

By using the BSE scheme, one can trace back the origin of the fine structure to the specific excited states. They can be analyzed by identifying the contributing transitions (*e*-*h* pairs), see Eq. (4). Let us now consider the excitations which constitute the edge peaks. The corresponding oscillator strengths for the respective AlN phases are compared in Fig. 2. Here the conduction-band minimum is set as zero. For the hexagonal wurtzite structure both components are shown, i.e., for the electric field of the x rays perpendicular and parallel to the *c* axis, respectively. In both cases, the edge peak consists of several bound core excitons, together with other excitations. For zinc blende, the situation is different. While the edge peak to a smaller degree consists of bound excitons, the states with the most pronounced oscillator strengths are found above the conduction-band minimum. In particular, the state with the highest oscillator strength is found directly above a gap located within the BSE absorption spectra. Turning to rs-AlN, the edge peak is due to the strongest bound core exciton, which here has the highest oscillator strength. In this case, the strength of the core-exciton edge peak is comparable to that of the Li-*K* edge in the wide band-gap insulator LiF.[12–14] For zb-AlN, there is a difference between both theoretical results and experiment at the very near-edge structure. While it can be argued to be small, it is still of interest to clarify its origin. One can think of several possible explanations. First, considering the experimental side, one may suspect the presence of aluminum oxide in the sample, as the peak position of Al-$L_{2,3}$ edge XANES of sixfold coordinated Al in Al_2O_3 is located at around 80 eV.[37] This is, however, not likely since the presence of such oxide films was not observed by TEM. Second, one could assign the discrepancy to the details of the underlying conduction-band structure. Indeed, we found the electronic bands to be sensitive to small changes in the lattice parameters. But also many-body effects could play a role. At present we only computed the Kohn-Sham bands without accounting for quasiparticle corrections. It needs to be clarified in the future whether better agreement with experiment could be achieved by employing the GW approximation.[54,55]

The wave functions of the most strongly bound excitons are visualized in Figs. 3(a)–3(c), each demonstrating one of

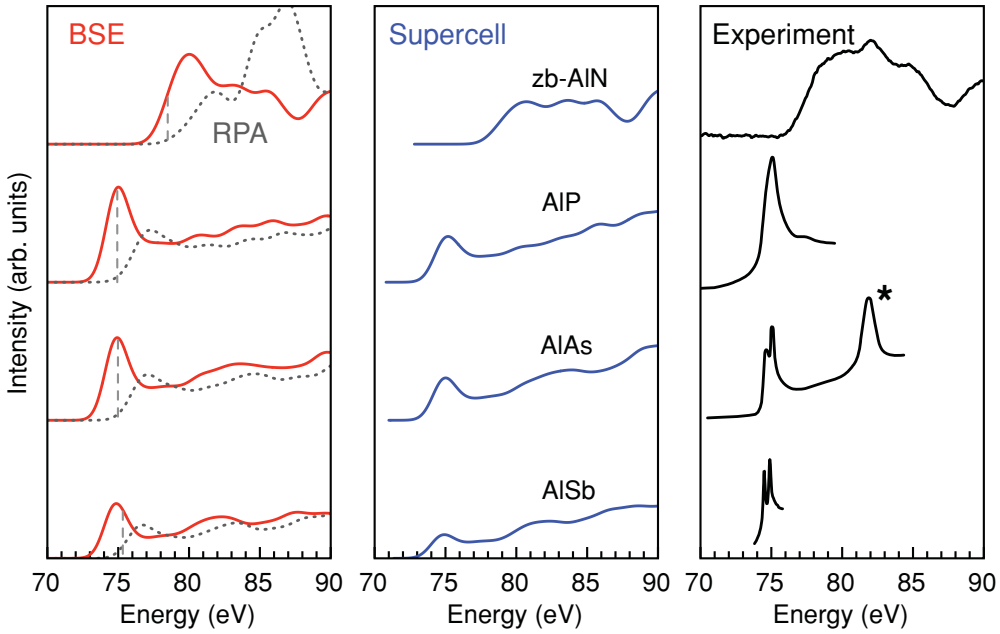

FIG. 4. (Color online) The near-edge absorption spectra for the Al-$L_{2,3}$ edge, from top to bottom: zb-AlN, AlP, AlAs, and AlSb. Results from BSE (red lines) and RPA (gray dotted lines) are collected in the left panel, supercell calculations with core hole are in the middle panel (blue lines), and experiment (black lines), AlAs and AlP (Ref. 60), AlSb (Ref. 61), in the right-hand panel. The dashed vertical lines in the first panel mark the respective conduction-band onsets. The experimental peak for AlAs marked with a star (*) is an artifact from the total electron yield XANES spectra, which is not obtained in the calculations.

the degenerate states for the respective AlN polymorph. In all cases, the core hole is fixed close to the selected Al atom, and directly located at the central Al atom in (b) and (c). On the left-hand side, the *absolute value* (modulus) of the respective wave function is considered. In all three cases, the isosurface corresponds to 1/15 of the maximum value. The three-dimensional (3D) contour plots on the right instead depict the *electron density* in specific lattice planes. They are chosen such that they visualize the peculiarities of the different structures. They also include the respective planes exhibiting the highest electron densities, which coincide with those containing the core hole (middle panels). The other planes go through the next-nearest nitrogen atoms (labeled N1 and N2, respectively).

For the wurtzite structure, Fig. 3(a), the excited electron probability density is high and localized at the nitrogen atom directly above the core-ionized Al atom (N2 plane). A high concentration is also found at the close-by N atoms below (N1 plane). In the Al plane, the density is prominent close to the hole and small at neighboring Al atoms. The asymmetries in the Al plane are due to the fact that only a single degenerate state is considered. Furthermore, the position of the hole is another source of symmetry breaking.

In Fig. 3(b) the situation for the zb lattice is illustrated. The three right panels show (111) planes through Al (middle) and nitrogen atoms, in front (N2) and behind (N1) of the Al (hole) plane. As in the case of wurtzite, a nitrogen atom (N2) is situated directly above the Al atom with the core hole. The excited electrons are not only localized at this Al site, but also at the N atoms closest to the hole and to some extent within the region in between. This is generally comparable to the results for the situation in the w structure (a), though the overall shape of the density is distinctively different as it exhibits a much wider extension in the zb case. Finally, in Fig. 3(c) the case of the rock-salt structure is shown. The displayed lattice planes are the same as in the previous case. The highest electron density is found directly at the core-hole site, with other sharp maxima in the neighboring nitrogen planes. Overall, the extension of the *e-h* wave function is somewhat delocalized along the Cartesian directions, as seen in the left panel.

B. AlP, AlAs, and AlSb

In this section, we study the Al $2p$ core excitations in the III-V semiconductors AlP, AlAs, and AlSb. AlAs is often used in GaAs-based devices in the zinc-blende structure, and Al-$L_{2,3}$ edge spectra have been measured in GaAs/AlAs/GaAs superstructures.[56–58] In AlSb, the Al-K edge has also been investigated experimentally.[59] The near-edge structures of AlP, AlAs, and AlSb are shown in Fig. 4 with zb-AlN included for comparison. Here, the BSE and RPA results are collected on the left-hand side, the supercell calculations in the middle panel, and experimental data, taken from Kelly *et al.*[60] and Johnson *et al.*,[61] on the right. As previously, all theoretical results are shifted for comparison with experiment, i.e., by 9.4, 9.2, and 9.3 eV for AlP, AlAs, and AlSb, respectively. (Note that these numbers again refer to the BSE results.) We predict the spectra for a wider energy range than covered by experiments.

The peak at 83 eV appearing in the total electron yield XANES spectra[60] for AlAs is most probably an experimental artifact, and thus not obtained in the calculations. In the experimental data for AlAs and AlSb, one can directly observe

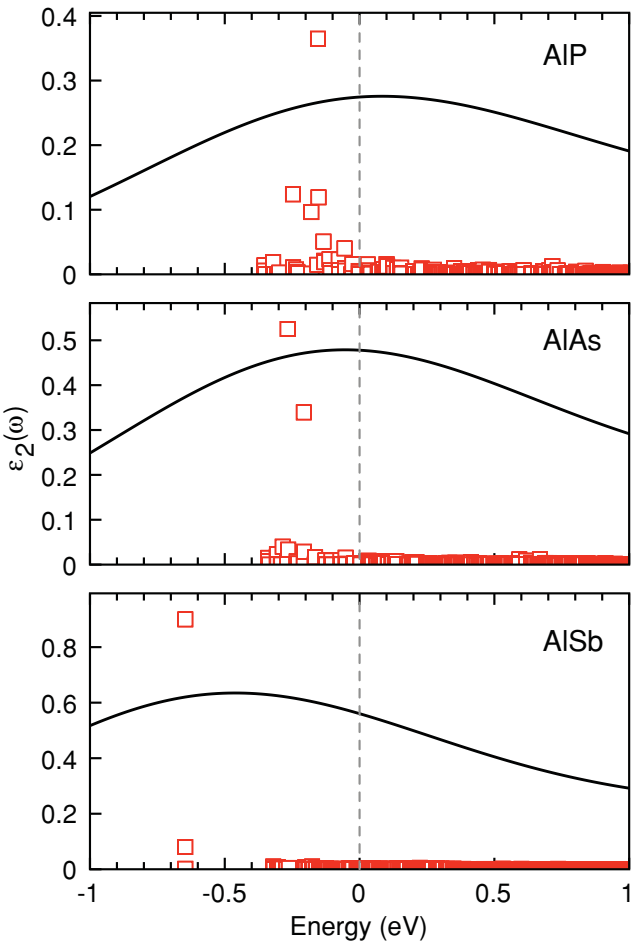

FIG. 5. (Color online) The oscillator strengths for the Al-$L_{2,3}$ edge excitations are shown (red boxes), from top to bottom, for AlP, AlAs, and AlSb. The conduction-band onset (dashed vertical lines) is set at zero energy. The absorption spectra (lines) are given to guide the eye, and are not in scale with the excitations.

the spin-splitting at the core edge. This is not reproduced in the calculations as we presently do not include spin-orbit coupling. The results are markedly different from the spectra of the AlN zinc-blende phase (Figs. 1 and 4). The energy of the core edge is clearly higher in zb-AlN, and this holds true also for the conduction-band minimum. The origin can be understood considering the band gap. In most ground-state calculations,[51,62] the indirect gap is obtained larger in zb-AlN than in the others. This difference can be explained in terms of the ionicity/covalency between Al and the anion. As the electronegativity is largest for N and smallest for Al, the character of the Al-N bond is more ionic than covalent in comparison with the other materials, thereby a stronger insulating behavior is expected. While the band structure of AlP, AlAs, and AlSb share many similar features,[62] that of zb-AlN is quite different.[51] As can be seen in Fig. 2, the metastable zinc-blende phase in AlN has a gap in the lower-energy conduction states, whereas AlP, AlAs, and AlSb do not exhibit such a feature.

Comparing the spectra of AlP, AlAs, and AlSb, there is a similarity between the compounds in the sense that there is a pronounced core-edge peak followed by a lower-intensity fine

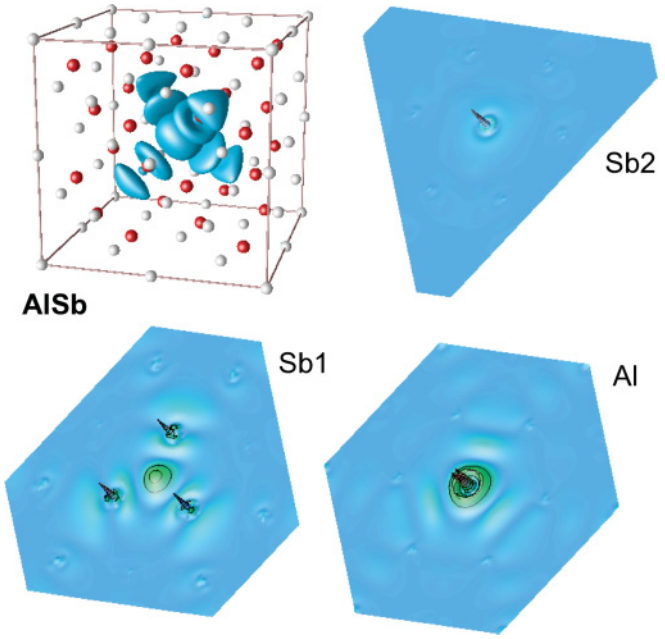

FIG. 6. (Color online) A strongly bound core exciton is visualized for the Al-$L_{2,3}$ edge in AlSb. The hole is situated at the Al atom in the center, and the absolute value (modulus) of the wave function is shown as isosurface in the lattice. Contour plots for three lattice planes depict the electron density in the central plane (Al) and nearest-neighbor planes (Sb1 and Sb2).

structure. There are differences, however, regarding details of the excitonic structure. Following the analysis made in the previous section, we study the excitations at the very near-edge structure in Fig. 5. For AlP and AlAs, the situation is akin to that of w- and zb-AlN, with the presence of several bound excitons and direct transitions which together constitute the peak at the edge. In the case of the Al-$L_{2,3}$ edge in AlSb, the situation is analogous to rs-AlN, as the core edge is completely dominated by a single strongly bound core-exciton state. A difference with rs-AlN is that the binding energy is smaller in this case.

In Fig. 6, the wave function of this strongly bound core exciton is given analogously to Fig. 3. The hole is fixed at the Al atom in the center. The electron is mostly localized to the direct vicinity of the hole, and to a lesser extent also close to the nearest-neighbor Sb atoms.

V. SUMMARY

We have carried out a *first-principles* study using the Bethe-Salpeter equation and supercell calculations within DFT employing the core-hole approximation to obtain the x-ray absorption near-edge structure spectra for the Al-$L_{2,3}$ edge in III-V semiconductors. The AlN-polymorphs in the wurtzite, zinc-blende, and rock-salt phases have been investigated, as well as AlP, AlAs, and AlSb, which all crystallize in the zb structure. In addition, we have presented electron energy-loss near-edge structure measurements of the AlN metastable zinc-blende phase. It is found that BSE gives a good description of relative intensities in the spectral features of the AlN structures. A difference between experiment and theory for the zinc-blende AlN near-edge fine structure is attributed to

the sensitivity of the absorption spectra on the details of the unoccupied bands. While the near-edge peak in rs-AlN and AlSb is due to a single strongly bound core exciton, it is a mixture of different excitations in the other materials.

ACKNOWLEDGMENTS

This study was carried out within the framework of a Grant-in-Aid for Scientific Research (A) and a Grant-in-Aid for Scientific Research on Priority Areas "Nano Materials Science for Atomic Scale Modification 474" from the Ministry of Education, Culture, Sports, Science and Technology (MEXT) of Japan. G.R. thanks Esteban Martinez-Guerrero and Bruno Daudin (CEA-Grenoble, INAC/SP2M, France) for providing the samples for cubic AlN. Financial support from the Austrian Science Foundation FWF and the European Theoretical Spectroscopy Facility (ETSF) is appreciated.

[1] I. Vurgaftman, J. R. Meyer, and L. R. Ram-Mohan, J. Appl. Phys. **89**, 5815 (2001).
[2] J. Stöhr, *NEXAFS Spectroscopy* (Springer-Verlag, Berlin, 1992).
[3] R. F. Egerton, *Electron Energy-loss Spectroscopy in the Electron Microscopy* (Plenum, New York, 1996).
[4] J. J. Rehr and R. C. Albers, Rev. Mod. Phys. **72**, 72 (2000).
[5] F. de Groot, Chem. Rev. **101**, 1779 (2001).
[6] I. Tanaka and T. Mizoguchi, J. Phys.: Condens. Matter **21**, 104201 (2009).
[7] T. Mizoguchi, W. Olovsson, H. Ikeno, and I. Tanaka, Micron **41**, 695 (2010).
[8] I. Tanaka, T. Mizoguchi, and T. Yamamoto, J. Am. Ceram. Soc. **88**, 2013 (2005).
[9] E. L. Shirley, Phys. Rev. Lett. **80**, 794 (1998).
[10] E. L. Shirley, J. Phys. Chem. Solids **61**, 445 (2000).
[11] J. A. Soininen and E. L. Shirley, Phys. Rev. B **64**, 165112 (2001).
[12] E. L. Shirley, J. Electron Spectrosc. Relat. Phenom. **137-140**, 579 (2004).
[13] W. Olovsson, I. Tanaka, P. Puschnig, and C. Ambrosch-Draxl, J. Phys.: Condens. Matter **21**, 104205 (2009).
[14] W. Olovsson, I. Tanaka, T. Mizoguchi, P. Puschnig, and C. Ambrosch-Draxl, Phys. Rev. B **79**, 041102R (2009).
[15] J. J. Rehr, J. A. Soininen, and E. L. Shirley, Phys. Scr. **T115**, 207 (2005).
[16] O. Wessely, M. I. Katsnelson, and O. Eriksson, Phys. Rev. Lett. **94**, 167401 (2005).
[17] P. Moreau, F. Boucher, G. Goglio, D. Foy, V. Mauchamp, and G. Ouvrard, Phys. Rev. B **73**, 195111 (2006).
[18] V. Mauchamp, M. Jaouen, and P. Schattschneider, Phys. Rev. B **79**, 235106 (2009).
[19] R. Laskowski and P. Blaha, Phys. Rev. B **82**, 205104 (2010).
[20] K. Jorissen and J. J. Rehr, Phys. Rev. B **81**, 245124 (2010).
[21] J. J. Rehr, J. J. Kas, F. D. Vila, M. P. Prange, and K. Jorissen, Phys. Chem. Chem. Phys. **12**, 5503 (2010).
[22] S.-P. Gao, C. J. Pickard, A. Perlov, and V. Milman, J. Phys.: Condens. Matter **21**, 104203 (2009).
[23] W.-Y. Ching and P. Rulis, J. Phys.: Condens. Matter **21**, 104202 (2009).
[24] C. Hébert, Micron **38**, 12 (2007).
[25] G. Onida, L. Rening, and A. Rubio, Rev. Mod. Phys. **74**, 601 (2002).
[26] L. J. Sham and T. M. Rice, Phys. Rev. **144**, 708 (1966).
[27] W. Hanke and L. J. Sham, Phys. Rev. B **12**, 4501 (1975).
[28] W. Hanke and L. J. Sham, Phys. Rev. Lett. **43**, 387 (1979).
[29] W. Hanke and L. J. Sham, Phys. Rev. B **21**, 4656 (1980).
[30] G. Strinati, Phys. Rev. Lett. **49**, 1519 (1982).
[31] G. Strinati, Phys. Rev. B **29**, 5718 (1984).
[32] [http://exciting-code.org].
[33] J. Vinson, J. J. Rehr, J. J. Kas, and E. L. Shirley, Phys. Rev. B **83**, 115106 (2011).
[34] R. Laskowski and N. E. Christensen, Phys. Rev. B **74**, 075203 (2006).
[35] R. Laskowski and N. E. Christensen, Phys. Status Solidi B **244**, 17 (2007).
[36] I. Tanaka and H. Adachi, Phys. Rev. B **54**, 4604 (1996).
[37] S.-D. Mo and W. Y. Ching, Phys. Rev. B **62**, 7901 (2000).
[38] T. Mizoguchi, I. Tanaka, M. Kunisu, M. Yoshiya, H. Adachi, and W. Y. Ching, Micron **34**, 249 (2003).
[39] T. Mizoguchi, I. Tanaka, S. Yoshioka, M. Kunisu, T. Yamamoto, and W. Y. Ching, Phys. Rev. B **70**, 045103 (2004).
[40] O. K. Andersen, Phys. Rev. B **12**, 3060 (1975).
[41] P. Blaha, K. Schwartz, G. Madsen, D. Kvasnicka, and J. Luitz, *WIEN2k An Augmented Plane Wave Plus Local Orbitals Program for Calculating Crystal Properties*, Vienna, Austria, 2001.
[42] P. Puschnig and C. Ambrosch-Draxl, Phys. Rev. B **66**, 165105 (2002).
[43] P. Puschnig and C. Ambrosch-Draxl, Phys. Rev. Lett. **89**, 056405 (2002).
[44] K. Hummer, P. Puschnig, and C. Ambrosch-Draxl, Phys. Rev. Lett. **92**, 147402 (2004).
[45] K. Hummer and C. Ambrosch-Draxl, Phys. Rev. B **71**, 081202R (2005).
[46] R. Laskowski, N. E. Christensen, G. Santi, and C. Ambrosch-Draxl, Phys. Rev. B **72**, 035204 (2005).
[47] R. W. G. Wyckoff, *Crystal Structures 1*, 2nd ed. (Interscience, New York, 1963).
[48] J. P. Perdew, K. Burke, and M. Ernzerhof, Phys. Rev. Lett. **77**, 3865 (1996).
[49] G. Ferro, J. Camassel, S. Juillaguet, C. Balloud, E. K. Polychroniadis, Y. Stoemenos, J. Dazord, H. Peyre, Y. Monteil, S. A. Ruchworth, and L. M. Smith, Semicond. Sci. Technol. **18**, 1015 (2003).
[50] Y. C. Cheng, X. L. Wu, J. Zhu, L. L. Xu, S. H. Li, and P. K. Chu, J. Appl. Phys. **103**, 073707 (2008).
[51] F. Litimein, B. Bouhafs, Z. Dridi, and P. Ruterana, New J. Phys. **4**, 64 (2002).
[52] M. Sennour and C. Esnouf, Acta Mater. **51**, 943 (2003).
[53] J. C. L. Bossé, M. Sennour, C. Esnouf, and H. Chermette, Ultramicroscopy **99**, 49 (2004).
[54] L. Hedin, Phys. Rev. **139**, A796 (1965).
[55] F. Aryasetiawan and O. Gunnarsson, Rep. Prog. Phys. **61**, 237 (1998).
[56] A. Agui, S. Shin, C. Wu, K. Shiba, and K. Inoue, Phys. Rev. B **59**, 10792 (1999).

[57] A. Agui, C. Sathe, J. Guo, J. Nordgren, S. Mankefors, P. Nilsson, J. Kanski, T. Andersson, and K. Karlsson, Appl. Surf. Sci. **166**, 309 (2000).

[58] S. Mankefors, P. O. Nilsson, J. Kanski, T. Andersson, K. Karlsson, A. Agui, C. Sathe, J. H. Guo, and J. Nordgren, Phys. Rev. B **61**, 5540 (2000).

[59] C. Sénémaud, A. Gheorghiu, and L. Ley, Phys. Rev. B **43**, 12413 (1991).

[60] M. K. Kelly, D. W. Niles, P. Perfetti, E. Colavita, A. Savoia, G. Margaritondo, and M. Henzler, Phys. Rev. B **32**, 5525 (1985).

[61] R. L. Johnson, J. H. Fock, L. Ley, and M. Cardona, in *Proceedings of the Seventeenth International Conference on the Physics of Semiconductors, 1984*, edited by D. J. Chadi and W. A. Harrsion (Springer, New York, 1985), p. 1239.

[62] A. H. Reshak and S. Auluck, Physica B **395**, 143 (2007).